# 3D model of the bronchial epithelial barrier to study repeated exposure to xenobiotics: Application to silver nanoparticles

Chloé Chivé, Claire Mc Cord, Daniel Sanchez-Guzman, Oliver Brookes, Prinitha Joseph, René Lai Kuen, Guillaume Phan, Armelle Baeza-Squiban, Stéphanie Devineau, Sonja Boland

Environmental Toxicology and Pharmacology 103 (2023) 104281

Contents lists available at ScienceDirect

Environmental Toxicology and Pharmacology

journal homepage: www.elsevier.com/locate/etap

# 3D model of the bronchial epithelial barrier to study repeated exposure to xenobiotics: Application to silver nanoparticles

Chloé Chivé [a,1,9], Claire Mc Cord [a,1], Daniel Sanchez-Guzman [a,2], Oliver Brookes [a,3], Prinitha Joseph [a], René Lai Kuen [b], Guillaume Phan [c,4], Armelle Baeza-Squiban [a,*,5], Stéphanie Devineau [a,6,7], Sonja Boland [a,6,8]

[a] Université Paris Cité, CNRS, Unit of Functional and Adaptive Biology, F-75013 Paris, France
[b] Université Paris Cité, INSERM UMS 025-CNRS UMS 3612, Faculté de Pharmacie, F-75006 Paris, France
[c] Institut de Radioprotection et de Sûreté Nucléaire (IRSN), PSE-SANTE/SESANE/LRSI - plateforme Paterson, F-92260 Fontenay-aux-Roses, France

ARTICLE INFO

Edited by Dr. M.D. Coleman

*Keywords:*
Nanotoxicology
Chronic toxicity
Calu-3
Secretome
Translocation
Metallothionein

ABSTRACT

There is still a lack of *in vitro* human models to evaluate the chronic toxicity of drugs and environmental pollutants. Here, we used a 3D model of the human bronchial epithelium to assess repeated exposures to xenobiotics. The Calu-3 human bronchial cell line was exposed to silver nanoparticles (AgNP) 5 times during 12 days, at the air-liquid interface, to mimic single and repeated exposure to inhaled particles. Repeated exposures induced a stronger induction of the metal stress response and a steady oxidative stress over time. A sustained translocation of silver was observed after each exposure without any loss of the epithelial barrier integrity. The proteomic analysis of the mucus revealed changes in the secreted protein profiles associated with the epithelial immune response after repeated exposures only. These results demonstrate that advanced *in vitro* models are efficient to investigate the adaptive response of human cells submitted to repeated xenobiotic exposures.

## 1. Introduction

The hazard assessment of chemicals is still mainly based on toxicological studies in animals. However, New Approach Methods (NAMs) are being developed to replace animal testing for ethical and economic reasons, and because data from animals are not always applicable to humans (Stucki et al., 2022). Regarding such methods, *in vitro* testing on human cells has made considerable progress, particularly with the introduction of validated tests for acute toxicity assessment, for example, to assess skin irritation (Bas et al., 2021). By contrast, few models are available to assess repeated exposures and long-term toxicity, although repeated and long-term exposures represent the most common exposure pattern in environmental toxicology. The main challenge to perform long-term toxicity studies *in vitro* is to maintain differentiated cultures on a long enough period to allow repeated exposures. This is not feasible with common 2D cultures, which favour proliferation at the expense of differentiation, and require frequent passages that can lead to cell selection (Xi et al., 2021). Moreover, epithelial cells do not reproduce the architecture and barrier function of a functional epithelium when they are cultured in 2D. As an alternative to 2D models, 3D models have been developed using two-compartment chambers with porous inserts to favour cell differentiation, cell-cell interactions and the formation of a tight epithelial barrier at the liquid-liquid or air-liquid interfaces (ALI) for intestinal, skin, or

* Corresponding author.
*E-mail address:* armelle.baeza@u-paris.fr (A. Baeza-Squiban).
[1] equal contributions
[2] ORCID: 0000-0002-7237-5931
[3] ORCID: 0000-0003-0074-8644
[4] ORCID: 0000-0001-7223-0559
[5] ORCID: 0000-0003-2403–8823
[6] equal contributions
[7] ORCID: 0000-0002-1133-5223
[8] ORCID: 0000-0002-4257-4104
[9] ORCID 0009-0008-8848-4770

https://doi.org/10.1016/j.etap.2023.104281
Received 9 June 2023; Received in revised form 14 September 2023; Accepted 20 September 2023
Available online 22 September 2023

pulmonary models (Lenz et al., 2013; Bauer et al., 2022).

In the case of lung models, repeated exposure of A549 and NCI-H441 alveolar cell models to engineered nanomaterials (NMs) was studied after 3 exposures at 24, 48, and 72 h by Meldrum et al. (Meldrum et al., 2022). Long-term exposure is also critical to assess the carcinogenic effect of NMs, from key molecular events to tumorigenesis. Yeyeodu et al. (2019) evaluated the long-term effects 7 days after a single exposure to Ag NMs of BEAS-2B (lung), MCF10AI (breast), and CCD-18Co (colon) epithelia. Wang et al. (2011) successfully exposed BEAS-2B lung epithelial cells to carbon nanotubes during 24 weeks and observed malignant transformation of the cells in 2D proliferating cell cultures (Wang et al., 2011). *In vitro* models of differentiated cells are needed for the risk assessment of repeated and long-term exposure to xenobiotics in order to fill the gap between acute *in vitro* toxicity tests and *in vivo* chronic toxicity studies. The MucilAir™ model of the differentiated primary bronchial epithelium was used by Di Cristo et al. to study repeated exposure to silica nanoparticles 5 days per week during 12 weeks to mimic occupational exposure (Di Cristo et al., 2020). Their results showed efficient epithelial defense mechanisms in agreement with *in vivo* data (Di Cristo et al., 2020). However, primary cultures show donor-specific responses leading to high variability between studies.

In this context, we have developed a 3D bronchial epithelium model for the assessment of repeated and long-term exposure that could be integrated into test batteries for the assessment of initiating molecular event and key events in specific adverse outcome pathways (AOP) of the respiratory system. Using the Calu-3 cell line cultured on inserts, we obtained a functional human bronchial epithelium model at ALI (Sanchez-Guzman et al., 2021). Calu-3 is derived from human lung adenocarcinoma and forms an epithelial barrier with tight junctions. It also produces mucus on the apical side (Grainger et al., 2006). Mucus hypersecretion or impaired mucus clearance are known in pulmonary diseases such as COPD, asthma, and lung cancers (Fahy and Dickey, 2010). Mucus secretion can also be stimulated by inhaled pollutants (Albano et al., 2022) and NMs such as titanium dioxide nanoparticles (Chen et al., 2011). This potential NM effect can be assessed on the Calu-3 bronchial epithelium model. Moreover, we showed that the apical secretome of differentiated Calu-3 cells is very similar to the one of human normal bronchial epithelial cells (NHBE) of healthy donors in terms of composition (Sanchez-Guzman et al., 2021). Braakhuis et al. also demonstrated the suitability of the Calu-3 cell line for repeated exposures, in contrast to other human bronchial cell lines (Braakhuis et al., 2020). The culture conditions were optimized to maintain a functional epithelium *in vitro* for at least 25 days and demonstrating a stable secretome composition over time (Sanchez-Guzman et al., 2021). These characteristics make this model suitable to study the repeated exposure to inhaled particles on a period of several weeks while keeping a well differentiated epithelium and a stable secretome composition. In this study, we exposed the bronchial epithelium to a model xenobiotic in order to test and validate this 3D model for the assessment of repeated toxicity. We chose silver nanoparticles (AgNPs) as a model NM in the context of the European BIORIMA project for the development of NAMs to assess the acute and chronic toxicity of NMs. Indeed, given the wide variety of NMs, testing all of them *in vivo* is not possible. It is therefore essential to develop relevant cellular models to go beyond the evaluation of NM acute toxicity. AgNPs are widely used as bactericidal components in numerous consumer products. They can be found in disinfectant sprays, masks and nasal sprays to treat and prevent lung infections, and in cosmetics (Raj et al., 2012). AgNPs are also used as fungicides to treat crops (Servin et al., 2015). These applications of AgNPs could result in repeated human exposure by inhalation. Several advanced *in vitro* models of alveolar barrier have already been used to evaluate AgNP toxicity but they were limited to single exposure (Herzog et al., 2014; Herzog et al., 2013; Motta et al., 2023).

The objective of this work was to set up an experimental strategy using our 3D model of human bronchial epithelium to evaluate the cellular response to repeated exposure to AgNPs at ALI. We performed 5 exposures to AgNPs at a single concentration of 10 μg/cm$^2$ every 2–3 days during 12 days. The epithelial response and the translocation of silver from the apical to the basal side were monitored after each exposure. A set of noninvasive tests was chosen to assess the impact of AgNPs on barrier integrity, pro-inflammatory response, and mucus secretion over time. The evolution of the apical secretome was analyzed after a single exposure and after 5 repeated exposures to AgNPs. This noninvasive strategy was completed by the analyses of gene expression after each exposure. The expression of genes involved in inflammatory response, mucus secretion, oxidative and metallic stresses were investigated. In addition, transmission electron microscopy (TEM) observations and inductively coupled plasma mass spectrometry (ICP-MS) assays were carried out to evaluate the internalization and translocation following repeated exposure of the epithelium.

## 2. Materials and methods

### 2.1. Characterization of AgNPs

NM-300 K AgNPs were provided by the European Joint Research Centre (JRC, Ispra, Italy). AgNPs are stabilized with 4% w/w polyoxyethylene glycerol trioleate and polyoxyethylene sorbitan monolaurate (European Commission et al., 2011). AgNP size and shape were characterized by Transmission Electron Microscopy (TEM), Dynamic Light Scattering (DLS), and Small Angle X-ray Scattering (SAXS). AgNPs diluted in milliQ $H_2O$ were deposited on a C Formvar grid and observed on a Jeol JEM-100S microscope (Jeol Ltd Tokyo, Japan) at 80 kV and 15, 000x. TEM images were acquired with Orius SC200 Gatan camera (Gatan-Roper Scientific, Evry, France). AgNP size distribution was measured by DLS in HBSS$^{Ca2+/Mg2+}$ (Gibco, France) at 37 °C with a Zetasizer Nano-ZS (Malvern Instruments, Ltd, Worcestershire, UK) at 0.01 mg/mL. This concentration is in the same range as the lowest concentration used for cell exposure (1 μg/cm$^2$ which corresponds to 20 μL of solution at 50 μg/mL). Each measurement was repeated 3 times. Two populations were identified with average hydrodynamic diameters of 4.5 ± 0.8 and 14.1 ± 0.5 nm respectively, in agreement with JRC results. The stability of AgNPs in Eagle's Minimum Essential Medium (MEM, Gibco, Life technologies, Courtaboeuf, France) supplemented with 4% fetal bovine serum (FBS, Sigma-Aldrich, Saint-Quentin Fallavier, France) was investigated in a previous study by Small X-Ray Angle Scattering (SAXS) to determine if dissolution occurs during the experiment time (Martin et al., 2022). An average diameter of 15.4 ± 0.2 nm was measured by SAXS and no dissolution was observed after incubation at 37 °C for 18 days. The acellular oxidative potential of AgNPs was determined by measuring the depletion of a set of antioxidants, uric acid (UA), ascorbic acid (AA), and reduced glutathione (GSH) by HPLC following incubation of AgNPs in a simplified synthetic respiratory tract lining fluid at 37 °C for 4 h according to (Crobeddu et al., 2020) (see detailed methods in supplementary information (SI).

### 2.2. Calu-3 cells

Human adenocarcinoma epithelial cells (ATCC® HTB-55™, LGC standard, Molsheim, France) were used from passage 27–34 according to (Sanchez-Guzman et al., 2021) (see detailed methods in SI).

### 2.3. Repeated exposure to AgNPs

0.5 mg/mL AgNPs were sonicated in HBSS$^{Ca2+/Mg2+}$ for 2 min x 2 on ice using a cup horn sonicator (450 W, 60 Hz, Branson, Ultrasonics corporation, Danbury, USA) at a sonication energy of 5.0 W. After sonication, AgNPs were diluted in HBSS$^{Ca2+/Mg2+}$ to deliver 1–10 μg AgNP per insert in the form of 4 × 5 μL droplets (20 μL total volume). Control cultures received 20 μL buffer. The treatment was repeated 5 times at D0, D2, D4, D7 and D9. 48 h after each treatment, the apical

surface was rinsed with 200 µL HBSS $^{Ca2+/Mg2+}$ to collect the apical secretome for analysis and to remove remaining AgNPs from the previous treatment. The theorical nominal AgNPs concentrations were 5 × 1 and 5 × 10 µg/cm$^2$ or 5 and 50 µg/cm$^2$ assuming that no AgNPs were removed by the rinsing.

### 2.4. Silver dosage by ICP-MS

Ag concentrations in the apical ($V_{HBSS}$ = 200 µL) and in the basal ($V_{MEM}$ = 1.5 mL) medium were measured after acidic dissolution of the samples after cell exposure to 1 and 10 µg/cm$^2$ at each time point. A solution of silver nitrate was used for external calibration (1000 mg/L Ag single element in 2% $HNO_3$, SPEX Certiprep, Horiba Jobin Yvon, Longjumeau, France). Bismuth nitrate (1000 mg/L $^{209}$Bi single element in 2% $HNO_3$, SPEX Certiprep) was added as an internal standard at 1 µg/L for Ag dosage by Inductively Coupled Plasma Mass Spectrometry (ICP-MS). For the analysis of Ag in culture media, HBSS and MEM samples corresponding to the apical and basal media respectively were homogenized using vortex shakers and diluted in 0.2 M nitric acid containing 1 µg/L Bi. A 100-fold dilution factor was applied to the MEM samples. A 500- and 50,000-fold dilutions were applied to the HBSS samples after cell exposure to 1 and 10 µg/cm$^2$ AgNPs respectively. Ag solubilisation was performed overnight at room temperature. The total Ag concentration was determined by direct measurement of 3 dilutions of each samples by ICP-MS (iCAP Q, Thermo Scientific, Courtaboeuf, France) coupled to a 1 mL FAST 4DX autosampler (Elemental Scientific, Omaha, Nebraska, USA) using both $^{107}$Ag and $^{109}$Ag. The external calibration range was prepared in 0.2 M nitric acid for each medium (HBSS or MEM) with the following $^{107}$Ag concentrations: 0, 0.001, 0.05, 0.1 and 0.5 µg/L. The results were expressed in counts per second and converted to µg. L$^{-1}$ of total Ag. Results are shown as mean ± standard deviation of 3 biological replicates. The Ag translocation was calculated as the ratio between the nominal silver concentration in the apical medium and the silver concentration measured in the basal medium after each exposure. Translocation was expressed in µg/L and as %. The cumulated Ag translocation was calculated as the sum of the percentage of translocation after each exposure.

### 2.5. Epithelial barrier integrity and cell viability

Epithelial barrier integrity was measured using the Trans-Epithelial Electrical Resistance (TEER) and Lucifer Yellow (LY) paracellular permeability assay. Cell viability was measured using AlamarBlue™ assay and Lactate Dehydrogenase (LDH) release in the culture medium using CytoTox 96® Non-Radioactive Cytotoxicity Assay (see detailed methods in SI).

### 2.6. ELISA and ELLA assays

Pro-inflammatory IL-6 and IL-8 cytokines were measured in apical and basal media using ELISA assays. The glycoprotein concentration in the apical secretome was measured using Enzyme-Linked Lectin Assay (ELLA) as described in a previous work (Sanchez-Guzman et al., 2021) (see detailed methods in SI).

### 2.7. RT-qPCR

RNA collection of control and treated cells was performed using Nucleospin RNA/Protein Mini kit (Macherey-Nagel, Hoerdt, France) following manufacturer's instructions (see Table S1 for the sequence of primers and detailed methods in SI).

### 2.8. Proteomics

The apical secretomes of control cells were analyzed at D2 and D11. The secretomes of treated cells were analyzed at D2 and D11 following single and repeated exposures to 10 µg/cm$^2$ AgNPs respectively. The apical secretomes collected in 200 µL HBSS were centrifuged at 14,000 g at 4 °C for 20 min to pellet AgNPs and the supernatants stored at − 80 °C. After trypsin digestion, samples were analyzed by quantitative LC-MS/MS on Orbitrap Fusion Tribrid mass spectrometer as described before (Sanchez-Guzman et al., 2021). Each analysis was performed in triplicate. Proteins were identified using MaxQuant and Andromeda (Cox et al., 2011). The search database used FASTA file on the *Homo sapiens* and *Bos taurus* from NCBI database (2021). The maximum number of missed cleavage and the false discovery rate were set to 2 and 0.01 respectively both for peptide and protein identification. Normalized label-free quantification was obtained with MaxLFQ algorithm in MaxQuant software. The proteomics data were analyzed with Perseus software (Tyanova et al., 2016) to exclude false positives. 3 additional selection criteria were applied to obtain the final protein list of human secreted proteins that were identified in at least 2 replicates. Heat maps were done with R software (v. 3.6.2) using the pheatmap feature (Kolde, 2019). The reactome pathway analysis was performed with g:Profiler using g:GOSt and g:SCS for the functional enrichment with a threshold of 0.5 (Raudvere et al., 2019). The complete list of proteins identified in the apical secretome of Calu-3 cells following repeated exposure to AgNPs or HBSS is available in the Excel file WS1.

### 2.9. TEM

Calu-3 cultures were fixed with 0.2 M sodium cacodylate, 2.5% glutaraldehyde and 2% paraformaldehyde, post-fixed with 1% osmium tetroxide and stained with 1% uranyl acetate according to Sanchez-Guzman et al. (2021). Semi-thin (500 nm) and ultrathin sections (80 nm) cut with a Leica Ultracut S microtome (Vienna, Austria) fitted with a diamond knife (Diatome ultra 45) were observed with a JEM-100S microscope (Jeol LtD Tokyo, Japan) and analysed with ImageJ software. Semi-thin sections were stained with toluidine blue (1%).

### 2.10. Statistical analysis

Statistical analysis were performed with GraphPad Prism (v.8.0). Data are expressed as mean ± SEM. Data were tested for normality with a Shapiro-Wilk test and multiple comparison two-way ANOVA corrected with Benjamini, Krieger and Yekutieli test were used. P-values $< 0.05$ were considered as statistically significant.

## 3. Results and discussion

To explore the potential of the 3D Calu-3 model in assessing repeated toxicity, we set up an original exposure protocol (Fig. 1) and used AgNPs as model NMs. Experiments performed on 2D Calu-3 cell cultures showed an inhibitory concentration ($IC_{50}$) of 20 µg/cm$^2$ for these nanoparticles, suggesting higher toxicity compared to other benchmark NMs tested within the European BIORIMA program. The stabilizers have no cytotoxic effect (Martin et al., 2022). AgNPs are thus a relevant positive control for model validation in this study. 3D Calu-3 cultures were grown at ALI for 7 days before the first treatment, as we have previously shown that this lag time was necessary to obtain a well differentiated mature bronchial epithelium (Sanchez-Guzman et al., 2021). Cultures were exposed 5 times to 10 µg/cm$^2$ AgNPs every 2–3 days (D0, D2, D4, D7, D9) giving a cumulative nominal dose of 50 µg/cm$^2$. The effects were analyzed 48 h after each exposure at D2, D4, D7, D9, and D11. Before each new treatment, the apical surface of the culture was rinsed with saline buffer (HBSS$^{Ca2+/Mg2+}$) to prevent AgNP accumulation and mimic mucociliary clearance occurring *in vivo*. However, not all the particles were removed because some are embedded in the mucus layer sticking to the cells, and others may interact with the cells. Exposure was performed by deposition of 4 droplets of a low volume of AgNP suspension (20 µL/insert) favouring

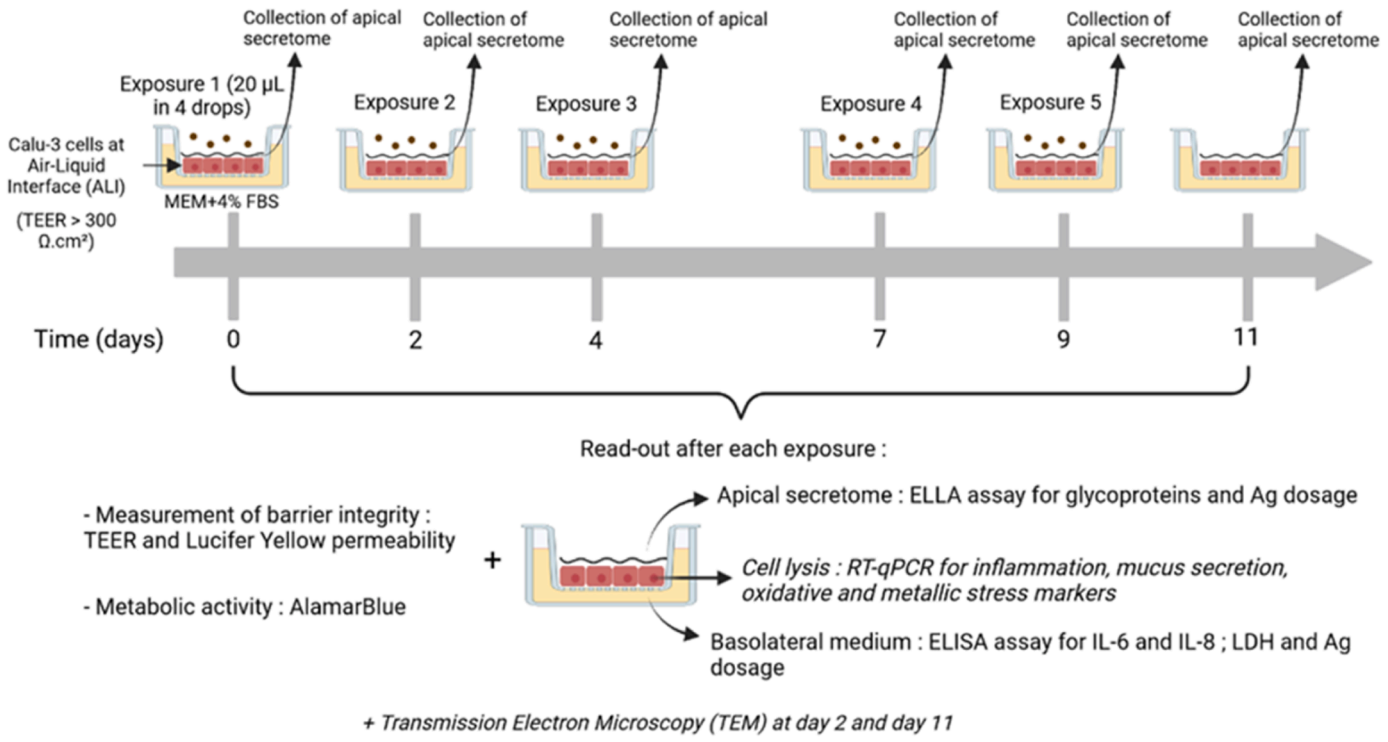


**Fig. 1.** Experimental design. The experiments were performed on Calu-3 cells at the Air-Liquid Interface (ALI) with TEER > 300 Ω.cm$^2$. Cultures were exposed 5 times at D0, D2, D4, D7, D9 at ALI to 20 µL HBSS (control cells) or 20 µL AgNPs at a concentration of 1–10 µg/cm$^2$ (treated cells). Before each exposure, the apical surface was rinsed with 200 µL HBSS $^{Ca2+/Mg2+}$ to recover the apical secretome. The effects of AgNPs were studied 48–72 h after each treatment (from D2 to D11). The barrier integrity was assessed by measuring the TEER and the LY permeability. The metabolic activity using the Alamar Blue assay. The apical secretome was collected to measure the glycoprotein concentration and for proteomic analysis. LDH release, IL-6 and IL-8 proinflammatory cytokine secretion were measured in the basal medium. Silver concentration was measured by ICP-MS in the apical and basal medium to evaluate Ag translocation. The cells were collected at D11 for mRNA extraction and RT-qPCR analysis of the expression of genes of interest. Some inserts were kept for TEM observations at D2 and D11.

NP deposition. This limited volume prevented detrimental effects of excessive apical liquid on the barrier integrity (SI Fig. S1). We selected a set of noninvasive endpoints to monitor the cellular effects of repeated exposure of the bronchial epithelium to AgNPs without collecting or sacrificing cells (Fig. 1). This noninvasive strategy was completed with the analysis of gene expression from D2 to D11, and cell fixation at D11 for TEM observation.

### 3.1. *Repeated exposure to AgNPs did not alter the permeability and viability of the Calu-3 barrier*

Noninvasive assays were performed to evaluate the cytotoxicity and the alteration of the barrier integrity induced by AgNPs during repeated exposure. The Alamar Blue (AB) assay, which measures the cell metabolic activity, did not show any significant difference in cell viability as a function of time in control cultures (Fig. 2A). AgNPs did not induce a significant decrease in cell viability regardless of the number of treatments. A moderate but significant stimulation of metabolic activity was observed after treatment, except at D7 for which a 72 h recovery period was observed before analysis, as opposed to 48 h for the other time points. This increase could be due to an hormesis effect, that is a stimulation of the biological response following exposure to a low concentration of a chemical that is reducing the cell activity at higher concentrations. A similar hormesis effect has been described for a 3D tetraculture of the alveolar barrier exposed to 20 nm AgNPs (Fizeşan et al., 2019) and for A549 cell culture exposed to AgNPs, and was related to increased expression of heme oxygenase 1 (*ho1*) (Sthijns et al., 2017). The release of lactate dehydrogenase (LDH), which is an indicator of membrane damage, was measured in the basolateral culture medium and no significant increase of LDH was observed in exposed cells compared to controls (Fig. 2B). These results show that 5 repeated exposures to AgNPs at 10 µg/cm$^2$ did not induce cytotoxicity in the Calu-3 bronchial epithelium model.

Then, we controlled the barrier integrity by measuring the Trans-Epithelial Electric Resistance (TEER) (Fig. 2C) and Lucifer Yellow (LY) permeability (Fig. 2D). In controls, a decrease of the TEER was observed, but values remained above 300 Ω.cm$^2$ throughout the experiment, which corresponds to TEER values of a tight epithelium. In treated cells, a slight and significant increase of TEER was observed at D2, D4, and D9. The LY permeability assay confirmed that no damage or loss of barrier integrity was observed, as LY values remained < 2% in all conditions. The threshold values of 300 Ω.cm$^2$ and 2% LY permeability were previously established for these culture conditions (Sanchez-Guzman et al., 2021). The same experiments were performed after 5 repeated exposures to 1 µg/cm$^2$ AgNPs. No cytotoxicity or alteration of the barrier integrity was observed (SI Fig. S2).

### 3.2. *AgNPs were internalized by epithelial cells without inducing ultrastructural alteration and Ag was translocated*

Cultures were fixed at D2 and D11 to determine whether AgNPs were internalized and induced ultrastructural modifications. Observations of semi-thin sections stained with toluidine blue allowing an overview of the barrier structure did not show any major alteration of the epithelial barrier (Fig. 3A), as suggested by cell viability and membrane permeability assays. Surprisingly, some cells were observed on the basal side of the insert membrane, a phenomenon that we did not observe when we established the model (Sanchez-Guzman et al., 2021). Due to a manufacturing disruption of Corning inserts, we moved from Transwell® to Millicell® inserts for this study. Their analysis by Raman microscopy showed that both inserts share the same chemical composition, polyethylene terephthalate (PET). The porosity of the inserts was further

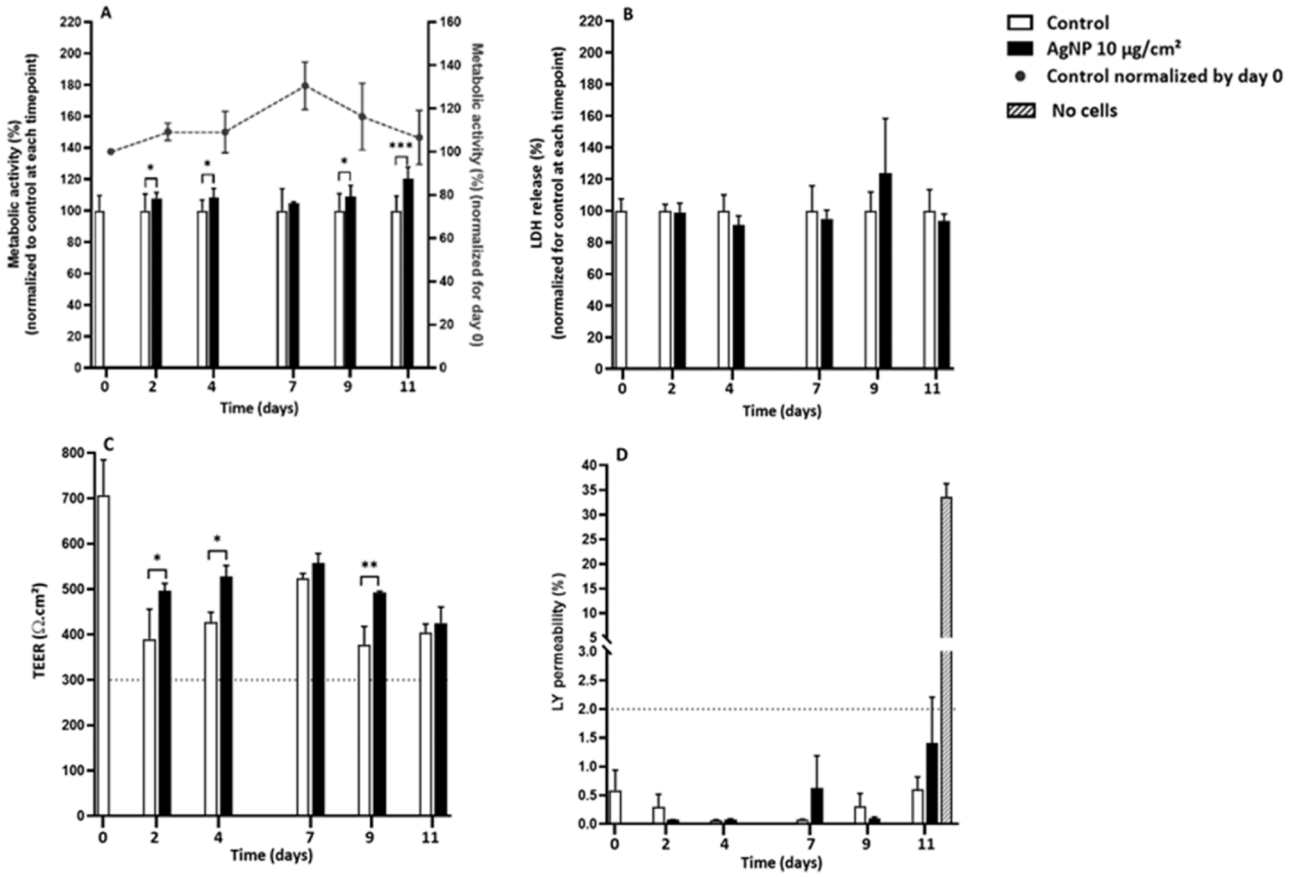


**Fig. 2.** Effect of 5 repeated exposures to AgNPs at 10 µg/cm$^2$ on Calu-3 viability and epithelial barrier integrity. Calu-3 epithelial barrier was exposed to HBSS $^{Ca2+/Mg2+}$ (control, white) or AgNPs (treated, black) from D0 to D9. The different endpoints were measured from D0 to D11. (A) Metabolic activity measured by the AlamarBlue assay (N = 6). Dotted lines represent the metabolic activity of the control culture during 12 days. (B) Cell membrane integrity measured by LDH release (N = 6). (C) Trans-epithelial electric resistance (TEER) (N = 2 D2-D9, N = 3 D0, D11). Minimal value for a tight barrier is indicated by a dotted line (TEER > 300 Ω.cm$^2$). (D) Lucifer Yellow (LY) permeability (N = 2 D2-D9, N = 3 D0, D11) of controls (white), treated cells (black), and empty insert (grey). Maximal value for a tight barrier is indicated by a dotted line (LY < 2%). *p < 0.05, ** p < 0.01, *** p < 0.001, significantly different from the control at the same time point.

characterized by Raman microscopy to analyze the pore morphology and to evaluate the percentage of single and fused pores in each insert (SI Fig. S3A-C). A significant percentage of fused pores with a diameter > 3 µm pore size was observed for each insert type (40% and 38% fused pores for Transwell® and Millicell® inserts respectively). These larger pores may facilitate cell crossing. A similar pore density was measured for both inserts with 16,000 and 14,000 pores/mm$^2$ for Transwell® and Millicell® inserts respectively. Raman microscopy as well as observations of semi-thin sections revealed that the pore wall of Millicell® inserts was smoother, while it is more irregular and crenelated for Transwell® (SI Fig. S3D-E), a feature that could favour cell crossing in Millicell® inserts. However, cell crossing seems limited after epithelial cell differentiation.

The ultrastructural observations of control and treated cells by TEM (SI Fig. 3B, S4) did not show any visible effect after repeated exposure to AgNPs. Tight junctions, desmosomes, and microvilli were well visible in both conditions. Cells contained mucus granules and normal organelle ultrastructures were observed. In treated cells, AgNPs embedded in the mucus were observed extracellularly on the apical side of the culture, suggesting that some particles may be trapped in the mucus layer. Particles were also observed inside cells, often in vesicles, suggesting AgNP endocytosis (Fig. 3B) as previously shown by Herzog et al. in a triple cell co-culture model (Herzog et al., 2014). As several membranes were observed in these vesicles, they could be autophagosomes.

The translocation of AgNPs through the epithelial barrier was investigated using cultures on TW (demonstrating no passage of cells to the basal side of the insert) by measuring total Ag concentration in the apical and basal medium after each exposure by ICP-MS (SI Fig. S5). Because the analysis requires acidic dissolution of the sample, both $Ag^+$ and AgNPs contribute to the total Ag concentration measured. Ag concentration in the apical medium increased between D2 and D9, suggesting that silver accumulated possibly due to decrease in cell uptake related to changes in mucus properties. The sum of the measured Ag concentration in the apical medium (163 mg/L) was lower than the nominal concentration (275 mg/L) corresponding to 5 repeated exposures at 10 µg/cm$^2$ (SI Table S2), confirming partial consumption of AgNPs between treatments by cell uptake. Significant Ag concentrations were detected in the basal medium from D2 to D9, which demonstrates Ag translocation after each exposure. The highest Ag concentration was measured at D2 (51 µg/L) in the basal compartment, showing that silver (in ionic or particulate form) could translocate through the epithelium following the first treatment. The cumulated translocation was evaluated to 103 µg/Lafter 4 exposures, corresponding to 0.09%, 0.03%, 0.05% and 0.01% of the nominal silver concentration applied to the apical compartment after 1, 2, 3 and 4 exposures respectively and a cumulated percentage of 0.19%. Even if the amount of silver inside cells could not be measured in this study, these data suggest that a fraction of AgNPs accumulate in the mucus layer where they could potentially be removed by mucociliary clearance especially as the concentration increases. Translocation results are also shown for 4 repeated exposures to 1 µg/cm$^2$ (SI Fig. S5). A similar trend was observed with Ag translocation observed after the first exposure. A cumulated translocation of 19 µg/L (0.34%) was measured. This decrease by a factor 5 compared to the experiment at high AgNP concentration is consistent with the

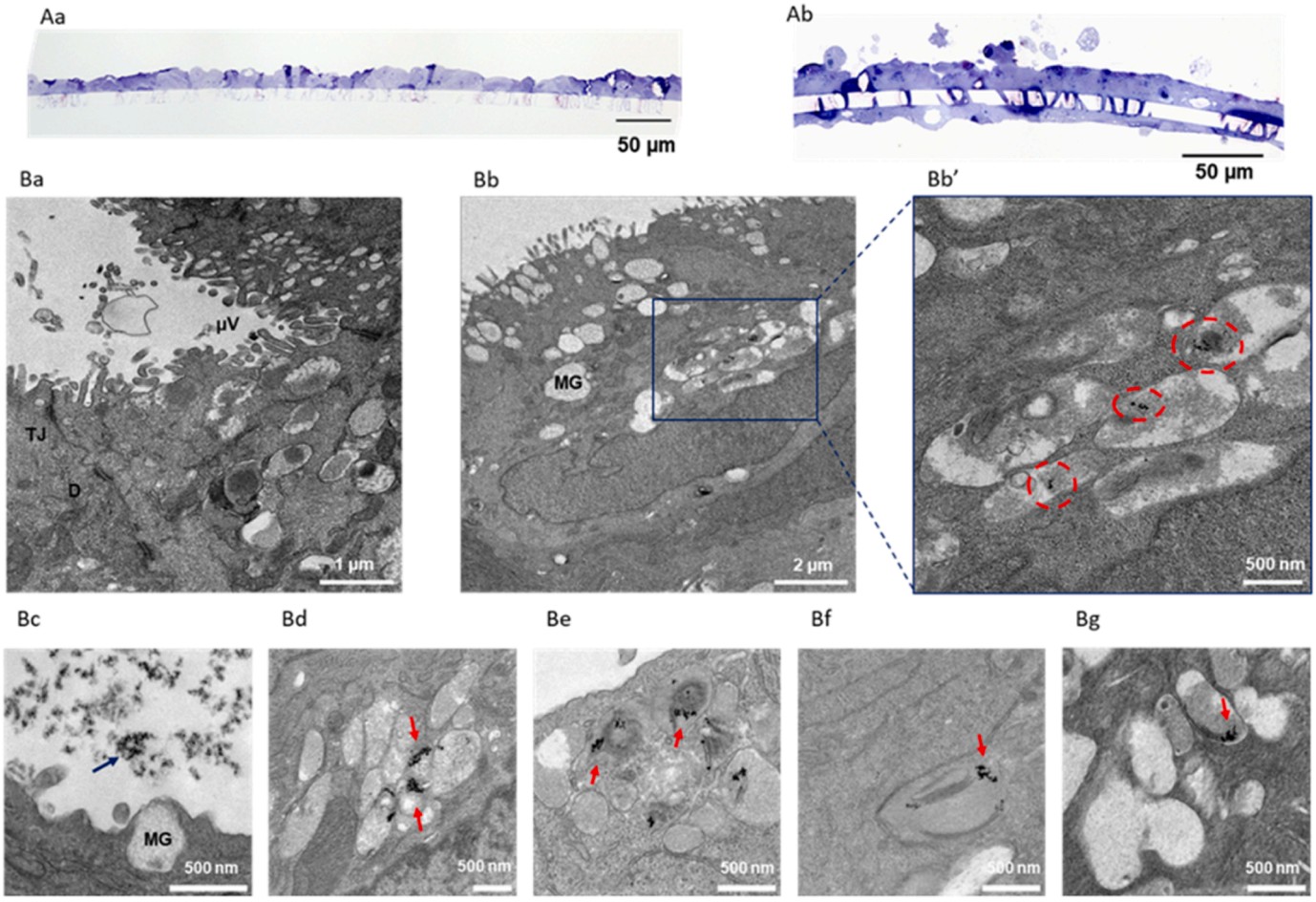


**Fig. 3.** Microscopy observations of Calu-3 sections. (A) Semi-thin sections of control cultures observed by optical microscopy, a: culture on Transwell insert, b: culture on Millicell insert. (B) Thin sections of treated cultures observed at D11 by TEM. Cells were exposed 5 times to AgNPs at 10 µg/cm$^2$. TJ: tight junctions, D: desmosome, MG: mucus granules, µV: microvillosities. Red arrows indicate AgNPs in cells. Blue arrows indicate AgNPs in mucus.

measured Ag concentration in the apical compartment (SI Table S2). These results clearly show that silver can cross the epithelial barrier. As the epithelium integrity is not compromised by AgNPs – tight junctions are preserved as shown by TEER and LY permeability – it suggests that translocation occurs by endocytosis of AgNPs followed by the release of $Ag^+$ and/or AgNPs on the basal side of the cells within 48 h.

The translocation of Ag measured on Calu-3 bronchial epithelium model is similar to values reported *in vitro* after a single exposure to AgNPs of human Caco-2 intestinal epithelium (0.5%) (Bouwmeester et al., 2011) and of human co-culture model of lung Calu-3 epithelial and EA.hy926 endothelial cells (1%) (Zhang et al., 2019). The penetration of AgNPs in the human nasal epithelium was also reported *ex vivo*, as well as Ag translocation through nasal epithelium model *in vitro* (Falconer et al., 2018), suggesting that a risk of silver translocation exists in case of exposure to AgNPs by inhalation at the different airway levels. We have shown that sustained silver translocation occurred without damage to the epithelial cells *in vitro*. However, other cell types present at the bronchial barrier could be affected due to possible intercellular trafficking of the particles, especially endothelial cells or dendritic cells which are in close contact with the epithelial cells.

### 3.3. AgNPs induced a pro-inflammatory response without mucus hypersecretion

In order to evaluate whether AgNPs induced a proinflammatory response, IL-6 and IL-8 proinflammatory cytokines were measured in the apical and basolateral media after each exposure. For an accurate interpretation of these data, the evolution of the constitutive release of these cytokines was first analyzed during the experimental time (12 days from D0 to D11) (Fig. 4). IL-8 was released in greater amount than IL-6 (15,000 pg and 600 pg respectively at D0) (Fig. 4A). Both apical and basal releases were observed for IL-6 and IL-8 (Fig. 4B-C). The release of IL-6 was polarized towards the apical side (70% of total secretion), whereas the release of IL-8 was equivalent in both orientations (Fig. 4B-C). The concentrations of IL-6 and IL-8 tended to increase with time in the apical medium in control cells, but they remained stable, except at D2, in the basal medium (SI Fig. S6).

Then, we checked whether cytokines adsorbed on AgNPs, which could interfere with the measurement of their concentration in treated cultures (SI Fig. S7). The results showed that AgNPs interfered with the ELISA assay. Therefore, we analyzed IL-6 and IL-8 release by treated cells only in the basal medium. Repeated exposures to 10 µg/cm$^2$ AgNPs induced a significant increase of IL-8 release in the basal medium regardless of the number of exposures, whereas no increase was observed following repeated exposure to 1 µg/cm$^2$ (Fig. 5A). It is interesting to note that other studies on ZnO toxicity showed that the addition of monocytes in the basal compartment could increase the release of cytokines (Bengalli et al., 2017). However, in a model of triculture including monocyte-derived macrophages and dendritic cells in addition to alveolar cells, Herzog et al. have not observed an increase in IL-8 release after ALI exposure to AgNPs at 3 µg/cm$^2$ (Herzog et al., 2014). Neither adaptation nor exacerbation of the pro-inflammatory response was observed after repeated exposures compared to single exposure to AgNPs. This may be due to the induction of protective

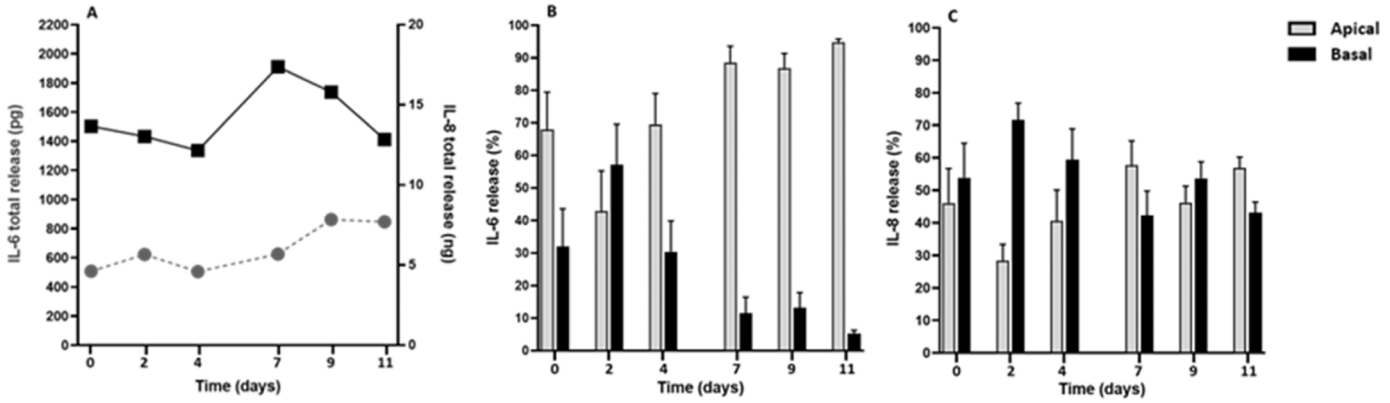


**Fig. 4.** Constitutive secretion of IL-6 and IL-8 cytokines by Calu-3 untreated cells. The apical and the basolateral secretomes were recovered from D0 to D11 to measure IL-6 and IL-8 secretions by ELISA. (A) Total secretion of IL-6 (left axis, pg, grey and round) and IL-8 (right axis, ng, black and square). (B-C) Percentage of apical and basal secretions of IL-6 (B) and IL-8 (C). (N = 3).

proteins such as metallothioneins and antioxidant proteins (see 2.4). Similar results were observed for IL-6 release in the basal medium to a lesser extent (Fig. 5B). The RT-qPCR results showed no increase in mRNA expression of these two cytokines (Fig. 5C-D).

Finally, mucus secretion was analyzed to determine whether AgNPs induced mucus hypersecretion. This potential NM effect was indirectly assessed using the ELLA assay that quantifies the glycoprotein content (as mucins are the most abundant glycoproteins in the secretome). The constitutive release of glycoproteins in the apical secretome remained constant during 12 days (Fig. 6). In treated cultures, a significant decrease of the glycoprotein concentration was observed after 3 and 4 exposures (17% and 14% decrease respectively). In order to determine whether this decrease was consistent with a reduction of mucin mRNA expression, MUC5AC expression that corresponds to mucin5ac, one of the main mucins, was analyzed. No significant change of MUC5AC expression was observed regardless of the number of treatments (SI Fig. S8). Repeated exposure to AgNPs resulted in decreased glycoprotein secretion either as a direct effect, as a result of upstream effects of AgNPs on gene expression, or due to recovery of the cultures between treatments.

### 3.4. AgNPs induced antioxidant and metal stress responses of the epithelial cells

To determine if oxidative stress is a toxicity pathway of AgNPs, we first evaluated the intrinsic oxidative potential of the particles by measuring the depletion in antioxidant molecules, ascorbic acid (AA), uric acid (UA), and gutathione (GSH), of a simplified lung lining fluid (Crobeddu et al., 2017). Little or no depletion of AA, UA, GSH (< 10%) was observed after 4 h incubation with AgNPs at concentrations up to 10 μg/mL at 37 °C (Online Resource Fig. S9). By contrast, high depletion of AA and GSH (100%) was observed for copper nanoparticles in the same conditions (SI Fig. S9). These results suggest that AgNPs used in this study have limited short term acellular oxidant effects compared to other metallic nanoparticles. To evaluate the cellular oxidative stress response, we measured after each exposure, the expression of heme oxygenase 1 (HO-1), an antioxidant enzyme expressed by Calu-3 cells and regulated by the Nrf2 (Nuclear factor erythroid 2-related factor 2) transcription factor (Fig. 7A). A significant induction of HO-1 was observed 48 h after each treatment, while no induction was observed 72 h after the 3rd treatment, suggesting a transient induction of HO-1 that is restored 72 h after exposure. HO-1 transient expression, which is typical of adaptive oxidative stress response, was previously observed in bronchial epithelial cells exposed to ambient particles (Val et al., 2011) as well as in a model of alveolar barrier exposed once to different types of AgNPs (Fizeșan et al., 2019).

In the case of metal stress, the adaptive cell response involves the activation of the metal regulatory transcription factor 1 (MTF1) that controls the expression of metallothioneins 1X (MT1X) and 2 A (MT2A) which will bind the metals that led to the activation of the transcription factor. MT1X and MT2A expressions were significantly induced in treated cells both 48 and 72 h post exposure (Fig. 7B-C) supporting observations done in a 3D tetraculture model of alveolar barrier exposed to different types of AgNPs at 5 μg/cm$^2$ for 6–24 h (Fizeșan et al., 2019). The increase of metallothionein expressions following consecutive exposures with a 48 h interval (D4 > D2, D11 > D9 > D7) and the lower level of induction observed after 72 h (D7 < D4) suggests that the induction of metallothioneins in epithelial cells leads to the successful sequestration of $Ag^+$ ions when the period between two successive treatments is long enough. As the induction of MT1X and MT2A was still significant at D7 compared to controls, we conclude that 72 h were not sufficient for cells to completely deal with the metal stress. Because the activation of MTF1 transcription factor requires binding of $Ag^+$ to MTF1 (Luther et al., 2012), this effect could be due to the slow dissolution kinetics of AgNPs after endocytosis.

The bronchial epithelium was exposed to silver nitrate ($AgNO_3$) to compare the effects of exposure to silver ions and AgNPs. Only one or two exposures were performed at D0 and D2 following the same protocol with an equivalent Ag concentration of 10 μg/cm$^2$. No effects after single or two repeated exposures to $AgNO_3$ on Calu-3 cell viability and barrier integrity were observed (SI Fig. S10A-C). We did not observe any induction of the expression of IL-6, IL-8, and MUC5AC (SI Fig. S10D-F). However, a significant induction of HO-1, MT1X, and MT2A expressions was observed (SI Fig. S10G-I). Our results are supporting those obtained in a model of tri-culture exposed for 24 h to $AgNO_3$ for IL-8 and HO-1 (Herzog et al., 2014). A stronger induction of metallothionein genes was observed following a single exposure to $AgNO_3$ compared to AgNPs. A lower induction was observed after the second exposure to $AgNO_3$ in contrary to AgNPs, which suggests that AgNP dissolution is involved in the delayed metal stress response observed in epithelial cells following multiple exposures. We have shown previously by SAXS analysis that AgNP dissolution in MEM is very limited after incubation for 18 days at 37 °C (Martin et al., 2022). Therefore, it is likely that AgNP dissolution occurs after endocytosis in the phagolysosomes observed by TEM, where dissolution would be favoured by low pH. The dissolution of AgNPs in lysosomes after endocytosis has been reported for different cell types *in vitro*. However, the dissolution kinetics of AgNPs depends on the particle shape, surface area, and capping or stabilizing agent, which in turn modulates the antioxidant and metal stress response of the cells (Graf et al., 2018; Smith et al., 2018; Gonzalez et al., 2015). It would be interesting to further study the respective contribution of Ag ions and particles in the toxic effects of AgNPs and the kinetics of their dissolution

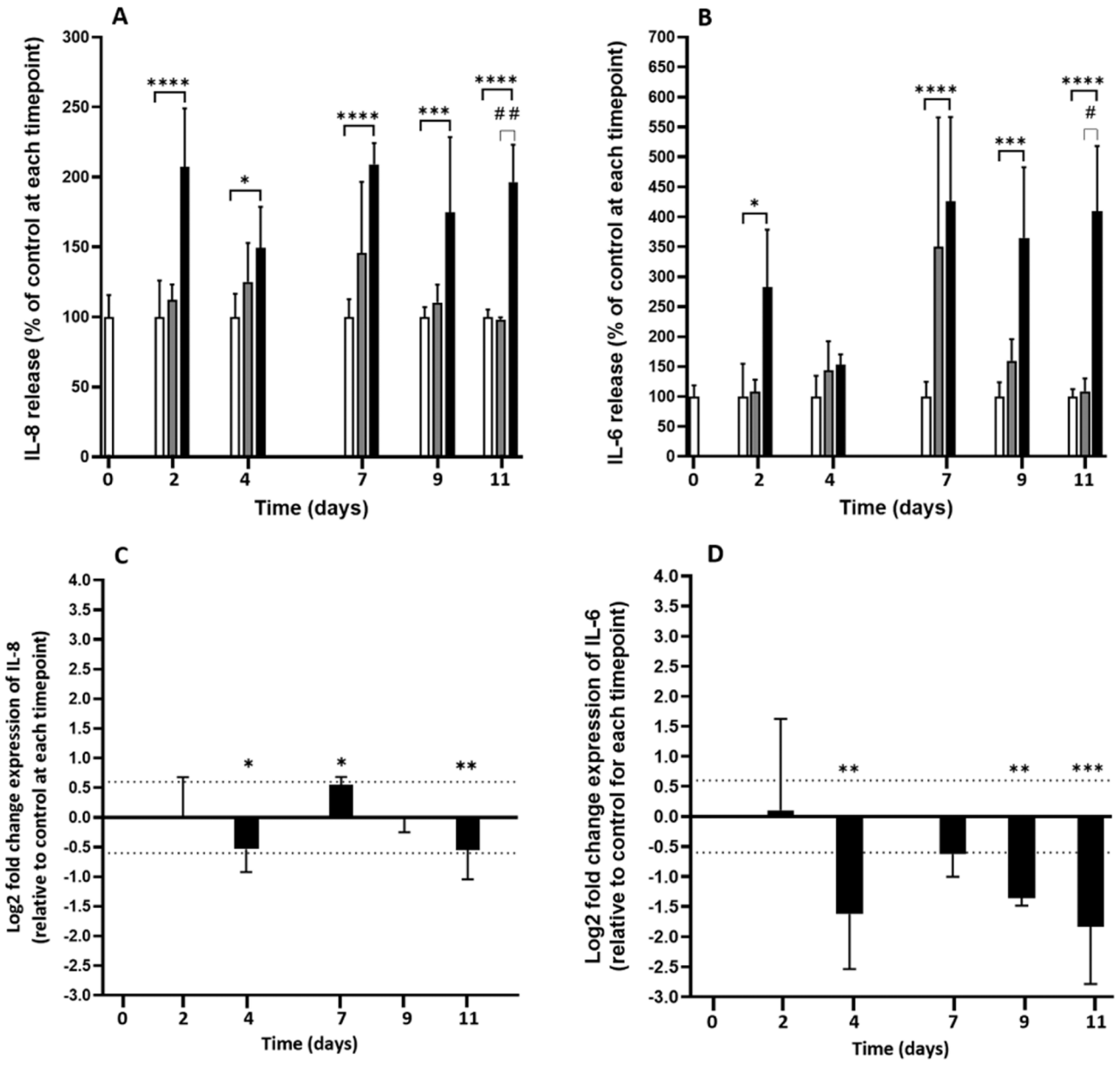


**Fig. 5.** Effect of 5 repeated exposures to AgNPs on the expression and secretion of IL-6 and IL-8 cytokines. Calu-3 epithelial barrier was repeatedly exposed to HBSS $^{Ca2+/Mg2+}$ (white), 1 μg/cm$^2$ AgNPs (grey) or 10 μg/cm$^2$ AgNPs (black) from D0 to D9. Concentrations of IL-8 (A) and IL-6 (B) in the basolateral secretome were measured by ELISA. (N = 4 for 1 μg/cm$^2$, N = 3 for 10 μg/cm$^2$). mRNA expression of IL-8 (C) and IL-6 (D) (N = 3). The dotted lines indicate fold changes considered significant. * $p < 0.05$, ** $p < 0.01$, *** $p < 0.001$, **** $p < 0.0001$, significantly different from control at the same time point.

in cells. This study aims to provide a suitable *in vitro* model for such studies on AgNPs toxicity as well as for other NPs.

### 3.5. Single and repeated exposure to AgNPs induced different changes in secretome composition

In addition to cytokines and mucins, Calu-3 cells secrete numerous proteins on their apical side, which contribute to the immune response and cell-to-cell communication of the bronchial epithelium (Sanchez-Guzman et al., 2021; Gupta et al., 2019). We analyzed the composition of the apical secretome of Calu-3 cells by quantitative proteomics to determine whether single and repeated exposure to AgNPs modulate the secretome composition, and whether these secreted proteins are involved in the cellular defense. The secretome composition was analyzed at D2 after a single exposure ('D2 AgNP') and at D11 after 5 repeated exposures ('D11 AgNP'), and compared to the secretomes of control cells at the same time points ('D2 Control', 'D11 Control') (Fig. 8). More than 500 extracellular proteins were identified in the apical secretome of Calu-3 cells, which is comparable to our previous results on the long-term evolution of the bronchial epithelium secretome (Sanchez-Guzman et al., 2021). The Principal Component Analysis (PCA) performed on the 4 conditions showed two separate clusters for D2 AgNP and D11 AgNP respectively, suggesting differences in the secretome after single or repeated exposure to AgNPs (Fig. 8A). The comparison with the secretome of control cells is shown as a Venn diagram (Fig. 8B). The secretomes of D2 Control and D2 AgNP share 432 common extracellular proteins, while 62 proteins are specifically secreted by cells exposed to AgNPs (12%), and 9 proteins are secreted by control cells only (2%). The secretomes of D11 Control and D11 AgNP share 463 common extracellular proteins, while 29 proteins are specifically secreted by cells exposed to AgNPs (6%), and 12 proteins are secreted by control cells only (2%). We conclude that AgNPs induced

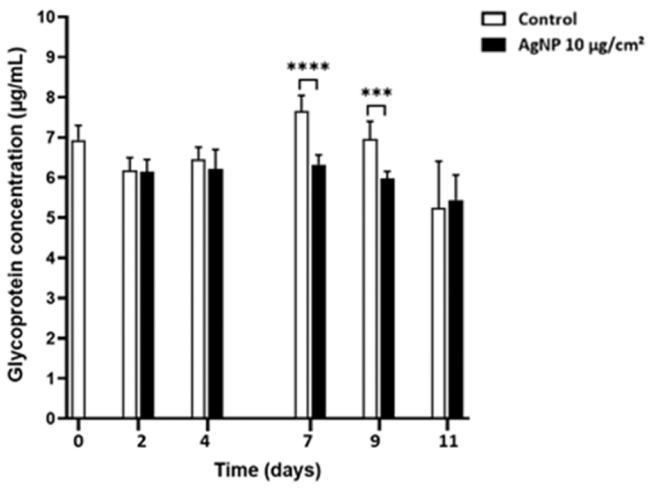


**Fig. 6.** Effect of 5 repeated exposures to AgNPs on the glycoprotein secretion and expression. Calu-3 epithelial barrier was repeatedly exposed to HBSS $^{Ca2+/Mg2+}$ or 10 µg/cm$^2$ AgNPs from D0 to D9. The apical secretomes were recovered from D0 to D11 to quantify glycoproteins by ELLA assay (N = 3). * $p < 0.05$, ** $p < 0.01$, *** $p < 0.001$, **** $p < 0.0001$, significantly different from control at the same time point.

secretion of specific proteins by epithelial cells at D2 and D11. The evolution of the secretome composition with time for control cells shows that 87% of the secreted proteins are common at D2 and D11 (SI Fig. S11A). Interestingly, when comparing proteins that are secreted by exposed cells only, we can see that 47 proteins are secreted at D2 AgNP only (62%), 14 proteins are secreted at D11 AgNP only (18%), and 15 proteins are common to D2 AgNP and D11 AgNP (20%) (Fig. 8C). The secretion of specific proteins following single exposure at D2 *versus* repeated exposure from D2 to D11 suggests adaptation of the epithelial cell response to AgNPs with time. This conclusion is supported by the observed difference between the secretome profiles of treated and untreated cells at D2 and D11 respectively (Fig. 8). The evolution of the epithelial secretion is indeed a combination of the cellular response to AgNPs at each time point, the adaptation of the cell layer to repeated exposures and the evolution of the proteome with time of culture (SI Fig. S11).

To further investigate this effect, the reactome enrichment pathways of the secretomes were analyzed after selecting proteins that were specifically expressed in treated cells at D2 and/or at D11 compared to control cells (Fig. 8D). The reactome enrichment pathways of the secretomes of untreated cells are shown for comparison at D2 and D11 in SI Fig. S13. Significant pathways ($p > 0.5$) identified in D11 AgNP were not expressed in D2 AgNP, namely apoptosis, programmed cell death, and suppression of autophagy. As no loss of cell viability was observed during AgNP exposure, it suggests that these processes could be related to the cellular turnover of the cellular layer by anoikis, which has already been observed with this model (Sanchez-Guzman et al., 2021). Secreted proteins involved in neutrophil degranulation were strongly expressed at D2, but not at D11, suggesting a stronger immune response after a single exposure.

The composition of the 20 most abundant proteins in the secretome of control and exposed cells was compared using a heat map to highlight differences in secreted protein abundancy and identify depleted or enriched proteins in the secretome after exposure to AgNPs (SI Fig. S11B). The heatmap of the full secretome is also provided in SI Fig. S12. α1-antichymotrypsin (*serpina3*) and galectin-3 binding protein (*lgals3bp*) proteins were enriched in the secretome of D2 AgNPs, suggesting enhanced enzymatic activity and immune response of the epithelium after exposure to AgNPs, while mucin 5AC (*muc5ac*) was depleted compared to control cells, in line with our observation on glycoprotein secretion. Polymeric immunoglobulin receptor (*pigr*) and immunoglobulin G (*fcgbp*) were both enriched in the secretome of D11 AgNPs, suggesting that epithelial immune response was also triggered after repeated exposure to AgNPs. The absence of *pigr* enrichment at D2 AgNP after a single exposure could be explained by the long-term evolution of the epithelium *in vitro*, as we observed before that this protein becomes more abundant in the mature secretome of Calu-3 cells (Sanchez-Guzman et al., 2021). By contrast, α1-antitrypsin (*serpina1*) was depleted in the secretome of D11 AgNP compared to D11 Control and D2 AgNP, suggesting that the enzymatic balance between proteases and protease inhibitors in the secretome may change after repeated exposure to AgNPs. The analysis of the secretome revealed changes in the secreted protein profiles associated with the epithelial immune response after multiple exposures to AgNPs that were unseen after a single exposure to the toxic compound of interest.

### 3.6. Advantages and limits of Calu-3 models for chronic toxicity studies

In this study, we used Calu-3 cell line to generate a human bronchial epithelial barrier. Calu-3 cells are commercially available, which is an advantage compared to NHBE (normal human bronchial epithelial cells), especially for screening different compounds or conditions. Primary cells from donors are available at higher cost and present high variability between individuals, which requires repeating the experiments with epithelia from different donors. In the context of the development of Integrated Approaches to Testing and Assessment (IATA), a low cost model present advantages when used in the first tier of tests to identify toxicity mechanisms, which can then be confirmed using NHBE models. The Calu-3 model was also used by Braakhuis et al. to study particle toxicity following aerosol exposure using a continuous airflow and an automated exposure system (Braakhuis et al., 2020). This

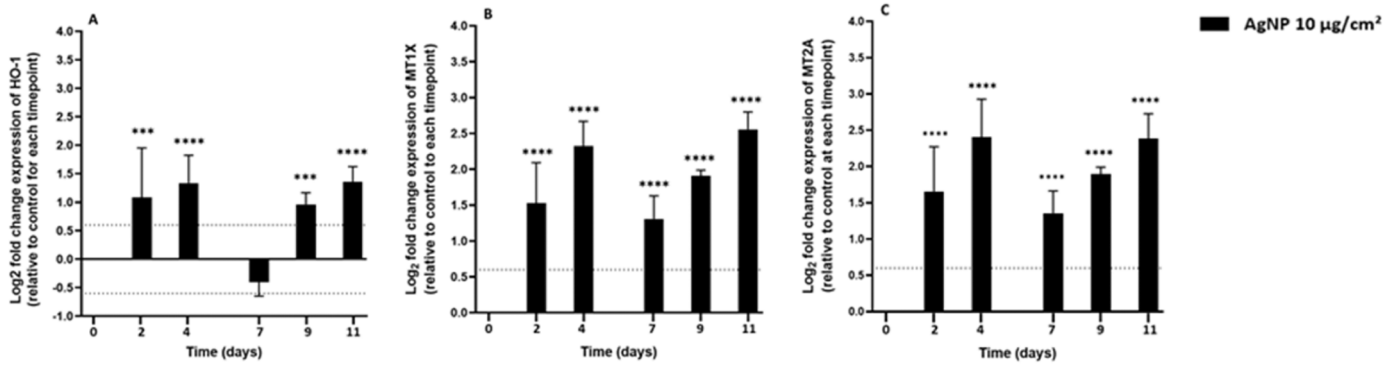


**Fig. 7.** Effect of 5 repeated exposures to AgNPs on the expression of heme oxygenase 1 and metallothioneins 1X and 2 A. Calu-3 epithelial barrier was repeatedly exposed to HBSS $^{Ca2+/Mg2+}$ or 10 µg/cm$^2$ AgNPs from D0 to D9. mRNA were extracted 48 h after each treatment (72 h for D7) to study (A) HO-1, (B) MT1X and (C) MT2A expression (N = 3). * $p < 0.05$, **$p < 0.01$, ***$p < 0.001$, ****$p < 0.0001$, significantly different from control at the same time point.

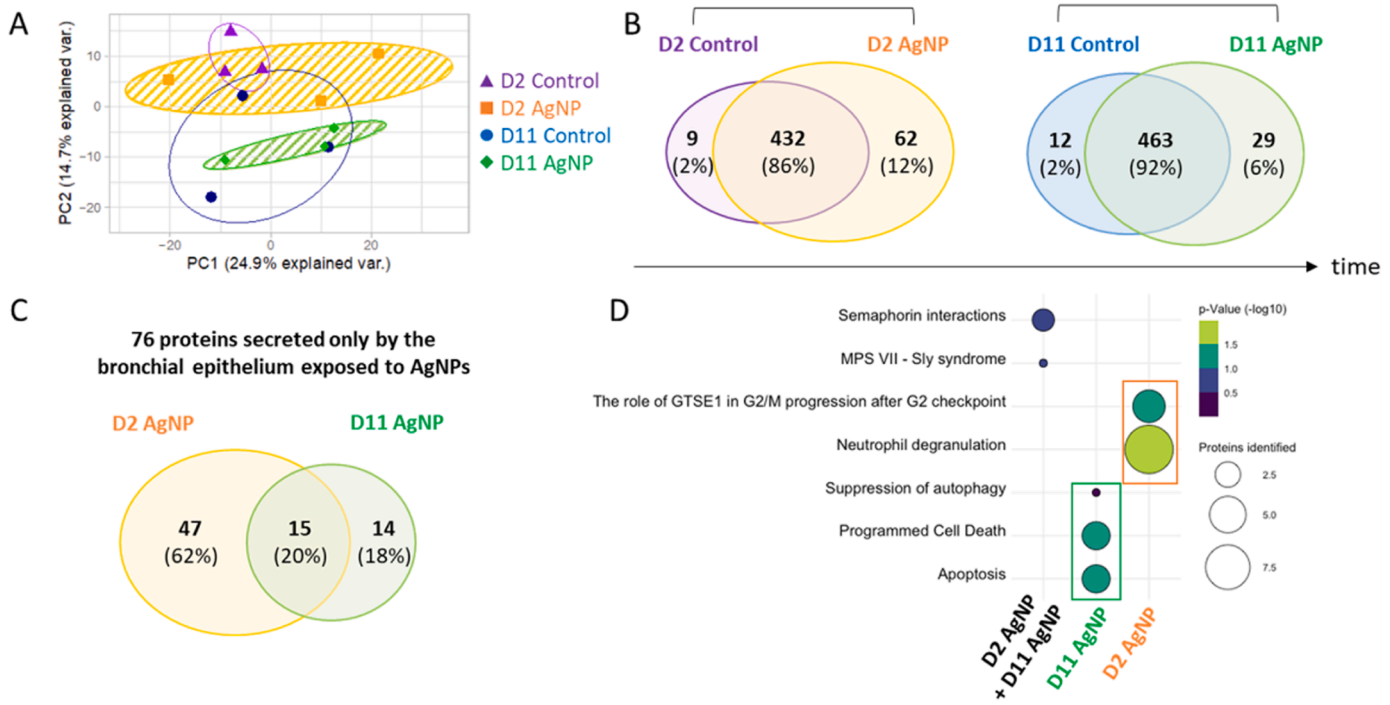


**Fig. 8.** Quantitative proteomic analysis of the apical secretome of Calu-3 cells after repeated exposure to AgNPs. Calu-3 epithelial barrier was repeatedly exposed to HBSS or 10 μg/cm$^2$ AgNPs from D0 to D9. (A) PCA analysis of the secreted protein composition and abundance at D2 and D11 for the control (open circles) and treated cells (hatched circles). (B) Time evolution of the secretome at D2 and D11 represented in a Venn diagram. Numbers of common and unique proteins between control and treated cells are shown for each time point. (C) Comparison of the proteins that are secreted by cells exposed to AgNPs only at D2 and D11. (D) Reactome enrichment pathways of the secreted proteins identified in cells exposed to AgNPs only. The 3 columns correspond to proteins common to D2 AgNP and D11 AgNP, proteins specific to D11 AgNP, and proteins specific to D2 AgNP respectively. The size and the colours of the symbols are associated to the number of proteins associated with a given pathway and the corresponding p-value ($p > 0.5$).

device reproduces realistic exposure conditions, but it requires expensive equipment. The aerosolization method is not applicable to all inhaled contaminants due to the heating process, which is not compatible with some organic materials or plastic particles. It proved to be possible for AgNPs (Fizeşan et al., 2019; Herzog et al., 2013) but was only demonstrated for single exposure. The nebulisation system will lead to a thin liquid layer on top of the epithelium of about 10 μm after a single exposure compared to around 180 μm with our exposure scenario. However, we demonstrate here that the pseudo-ALI method we used allowed 5 repeated exposures without any damage to the epithelial barrier. One experiment was performed with 12 repeated exposures during 28 days to reproduce *in vitro* the sub-acute toxicity experiments performed during 28 days *in vivo* (data not shown). Our results also highlight the importance of the insert membrane choice to limit cell crossing. This simple and low-cost model compared to primary cell cultures can be easily used by laboratories to address the issue of chronic toxicity.

Using this model, we assessed the toxicity of AgNPs on the bronchial epithelium following repeated exposures during 12 days. Our study completes previous studies performed using single exposure with AgNPs either with 2D or advanced 3D co-culture models mimicking the alveolar barrier (Fizeşan et al., 2019; Herzog et al., 2013; Motta et al., 2023). Primary bronchial epithelial cells in 3D cultures could also be used to perform repeated exposures but these commercially available models present huge donor variability. Organoids using primary cells also allow long-term cultures and hepatic organoids have been succesfully used for repeated exposure to AgNPs (Kermanizadeh et al., 2014) but present the same difficulty of donor variability. Other studies on chronic toxicity of NPs have thus used cell lines by subculturing the cells once a week (Comfort et al., 2014; Vales et al., 2015). The advantage of our culture model using Calu-3 is that this cell line proliferates very slowly and does not grow in layers (Sanchez-Guzman et al., 2021). This cell line was also recently used for 3D bioprinting to study NP toxicity (Gerbolés et al., 2023). In a previous study we compared the secretome profile of Calu-3 cell line model and primary human bronchial epithelial cells (Mucilair™) during 18 days, corresponding to a time-window compatible with repeated exposures to any type of xenobiotic (Sanchez-Guzman et al., 2021). We identified more than 400 extracellular proteins in the apical secretome of Calu-3 and primary cells and observed a high degree of similarity in the epithelial cell secretome in the Calu-3 and Mucilair™ models. We observed a pro-inflammatory, antioxidant and metal stress responses *in vitro* that is consistent with in *vivo* data. Neutrophil infiltration of the bronchoalveolar lavage of mice (Stebounova et al., 2011) or rats (Braakhuis et al., 2014) was observed after AgNP inhalation for 2 weeks and 4 days respectively. Moderate inflammation with lung damage and transient neutrophil infiltration was already shown after a single intratracheal instillation of mice to AgNPs (Kaewamatawong et al., 2014). It was associated to oxidative stress and metal stress with the induction of superoxide dismutase and metallothioneins in alveolar cells, in a transient manner which is consistent with the results obtained in this study. AgNP internalization observed here was also reported *in vivo* in lung epithelial cells (Braakhuis et al., 2014; Sung et al., 2009).

Our model allowed us to observe *in vitro* transient effects and epithelial cell responses that are increased with multiple exposures. This model is thus well adapted to study the adaptive response of the epithelium to repeated and long-term exposure to pollutants. As *in vitro* responses after repeated exposure to AgNPs are consistent with *in vivo* observations, it demonstrates the suitability and reliability of this model for toxicology studies.

## Funding

This project received funding from the European Union's Horizon 2020 research and innovation program under Grant agreement no.

760928 (BIORIMA). D.S.G. was supported by a fellowship from the Ecole Doctorale Médicaments, Toxicologie, Chimie, Imageries, Université Paris Cité.

## CRediT authorship contribution statement

**A.B.S.**, **S. B.** and **S. D.** contributed to the study conception and design. Material preparation, data collection and analysis were performed by all authors. The first draft of the manuscript was written by **C. C.**, **A.B.S.**, and **S.D.** All authors commented on previous versions of the manuscript. All authors read and approved the final manuscript.

## Declaration of Competing Interest

The authors declare that they have no known competing financial interests or personal relationships that could have appeared to influence the work reported in this paper.

## Data Availability

Data will be made available on request. The datasets generated during and/or analysed during the current study are available from the corresponding author on reasonable request. The mass spectrometry proteomics data have been deposited to the ProteomeXchange Consortium via the PRIDE partner repository PXD042088. Additionally, the complete protein lists can be found in the Excel file WS1, which is included in the Supplementary Information.

## Acknowledgments

We thank M. Alexandre Legrand, Ms. Clara Bariteau and Ms. Sabine Lam for their help with the ICP-MS analysis at the Institut de Radioprotection et de Sûreté Nucléaire (IRSN). We thank Ms. Charlotte Izabelle for her help on TEM observation of cells. This project received funding from the European Union's Horizon 2020 research and innovation program under Grant agreement no. 760928 (BIORIMA). C.C. was supported by the BIORIMA program. D.S.G. was supported by a fellowship from the Ecole Doctorale MTCI, Université Paris Cité. We acknowledge the Raman-AFM Platform (MPQ, Université Paris Cité) funded by ANR-18-IDEX-0001, IdEx Université Paris Cité.

## Appendix A. Supporting information

Supplementary data associated with this article can be found in the online version at doi:10.1016/j.etap.2023.104281.

## References

Albano, G.D., Montalbano, A.M., Gagliardo, R., Anzalone, G., Profita, M., 2022. Impact of air pollution in airway diseases: role of the epithelial cells (Cell Models and Biomarkers). IJMS 23 (5), 2799. Mar 3.

Bas, A., Burns, N., Gulotta, A., Junker, J., Drasler, B., Lehner, R., et al., 2021. Understanding the development, standardization, and validation process of alternative in vitro test methods for regulatory approval from a researcher perspective. Small 17 (15), 2006027 (Apr).

Bauer, M., Metzger, M., Corea, M., Schädl, B., Grillari, J., Dungel, P., 2022. Novel 3D-printed cell culture inserts for air–liquid interface cell culture. Life 12 (8), 1216. Aug 10.

Bengalli, R., Gualtieri, M., Capasso, L., Urani, C., Camatini, M., 2017. Impact of zinc oxide nanoparticles on an in vitro model of the human air-blood barrier. Toxicol. Lett. 279, 22–32.

Bouwmeester, H., Poortman, J., Peters, R.J., Wijma, E., Kramer, E., Makama, S., et al., 2011. Characterization of translocation of silver nanoparticles and effects on whole-genome gene expression using an *In Vitro* intestinal epithelium coculture model. ACS Nano 5 (5), 4091–4103. May 24.

Braakhuis, H.M., Gosens, I., Krystek, P., Boere, J.A., Cassee, F.R., Fokkens, P.H., et al., 2014. Particle size dependent deposition and pulmonary inflammation after short-term inhalation of silver nanoparticles. Part Fibre Toxicol. 11 (1), 49 (Dec).

Braakhuis, H.M., He, R., Vandebriel, R.J., Gremmer, E.R., Zwart, E., Vermeulen, J.P., et al., 2020. An air-liquid interface bronchial epithelial model for realistic, repeated inhalation exposure to airborne particles for toxicity testing. JoVE (159), 61210. May 13.

Chen, E.Y.T., Garnica, M., Wang, Y.-C., Chen, C.-S., Chin, W.-C., 2011. Mucin secretion induced by titanium dioxide nanoparticles. In: Wanunu, M. (Ed.), PLoS ONE 6 (1), e16198. Jan 19.

Comfort, K.K., Braydich-Stolle, L.K., Maurer, E.I., Hussain, S.M., 2014. Less Is More: Long-Term *in Vitro* exposure to low levels of silver nanoparticles provides new insights for nanomaterial evaluation. ACS Nano 8 (4), 3260–3271. Apr 22.

Cox, J., Neuhauser, N., Michalski, A., Scheltema, R.A., Olsen, J.V., Mann, M., 2011. Andromeda: a peptide search engine integrated into the MaxQuant environment. J. Proteome Res. 10 (4), 1794–1805 (Apr).

Crobeddu, B., Aragao-Santiago, L., Bui, L.-C., Boland, S., Baeza Squiban, A., 2017. Oxidative potential of particulate matter 2.5 as predictive indicator of cellular stress. Environ. Pollut. 230, 125–133 (Nov).

Crobeddu, B., Baudrimont, I., Deweirdt, J., Sciare, J., Badel, A., Camproux, A.-C., et al., 2020. Lung antioxidant depletion: a predictive indicator of cellular stress induced by ambient fine particles. Environ. Sci. Technol. 54 (4), 2360–2369. Feb 18.

Di Cristo, L., Boccuni, F., Iavicoli, S., Sabella, S., 2020. A human-relevant 3D in vitro platform for an effective and rapid simulation of workplace exposure to nanoparticles: silica nanoparticles as case study. Nanomaterials 10 (9), 1761. Sep 6.

European Commission. Joint Research Centre. Institute for Health and Consumer Protection., European Commission. Joint Research Centre. Institute for Environment and Sustainability., European Commission. Joint Research Centre. Institute for Reference Materials and Measurements. NM-Series of representative manufactured nanomaterials:NM 300 silver characterisation, stability, homogeneity. [Internet]. LU: Publications Office; 2011 [cited 2023 Apr 9]. Available from: https://data.europa.eu/doi/10.2788/23079.

Fahy, J.V., Dickey, B.F., 2010. Airway mucus function and dysfunction. N. Engl. J. Med 363 (23), 2233–2247. Dec 2.

Falconer, J.L., Alt, J.A., Grainger, D.W., 2018. Comparing ex vivo and in vitro translocation of silver nanoparticles and ions through human nasal epithelium. Biomaterials 171, 97–106 (Jul).

Fizeșan, I., Cambier, S., Moschini, E., Chary, A., Nelissen, I., Ziebel, J., et al., 2019. In vitro exposure of a 3D-tetraculture representative for the alveolar barrier at the air-liquid interface to silver particles and nanowires. Part Fibre Toxicol. 16 (1), 14.

Gerbolés, A.G., Galetti, M., Rossi, S., Lo Muzio, F.P., Pinelli, S., Delmonte, N., et al., 2023. Three-Dimensional Bioprinting of Organoid-Based Scaffolds (OBST) for long-term nanoparticle toxicology investigation. IJMS 24 (7), 6595. Apr 1.

Gonzalez, L., De Santis Puzzonia, M., Ricci, R., Aureli, F., Guarguaglini, G., Cubadda, F., et al., 2015. Amorphous silica nanoparticles alter microtubule dynamics and cell migration. Nanotoxicology 9 (6), 729–736. Aug 18.

Graf, C., Nordmeyer, D., Sengstock, C., Ahlberg, S., Diendorf, J., Raabe, J., et al., 2018. Shape-dependent dissolution and cellular uptake of silver nanoparticles. Langmuir 34 (4), 1506–1519.

Grainger, C.I., Greenwell, L.L., Lockley, D.J., Martin, G.P., Forbes, B., 2006. Culture of Calu-3 cells at the air interface provides a representative model of the airway epithelial barrier. Pharm. Res. 23 (7), 1482–1490 (Jul).

Gupta, R., Radicioni, G., Abdelwahab, S., Dang, H., Carpenter, J., Chua, M., et al., 2019. Intercellular communication between airway epithelial cells is mediated by exosome-like vesicles. Am. J. Respir. Cell Mol. Biol. 60 (2), 209–220 (Feb).

Herzog, F., Clift, M.J., Piccapietra, F., Behra, R., Schmid, O., Petri-Fink, A., et al., 2013. Exposure of silver-nanoparticles and silver-ions to lung cells in vitro at the air-liquid interface. Part Fibre Toxicol. 10 (1), 11 (Dec).

Herzog, F., Loza, K., Balog, S., Clift, M.J.D., Epple, M., Gehr, P., et al., 2014. Mimicking exposures to acute and lifetime concentrations of inhaled silver nanoparticles by two different in vitro approaches. Beilstein J. Nanotechnol. 5, 1357–1370. Aug 26.

Kaewamatawong, T., Banlunara, W., Maneewattanapinyo, P., Thammachareon, C., Ekgasit, S., 2014. Acute and subacute pulmonary toxicity caused by a single intratracheal instillation of colloidal silver nanoparticles in mice: pathobiological changes and metallothionein responses. J. Environ. Pathol. Toxicol. Oncol. 33 (1), 59–68.

Kermanizadeh, A., L Hr, M., Roursgaard, M., Messner, S., Gunness, P., Kelm, J.M., et al., 2014. Hepatic toxicology following single and multiple exposure of engineered nanomaterials utilising a novel primary human 3D liver microtissue model. Part Fibre Toxicol. 11 (1), 56 (Dec).

Kolde R. Pheatmap: Pretty Heatmaps. R package version 1.0.12. 1–8. 2019.

Lenz, A.-G., Karg, E., Brendel, E., Hinze-Heyn, H., Maier, K.L., Eickelberg, O., et al., 2013. Inflammatory and oxidative stress responses of an alveolar epithelial cell line to airborne zinc oxide nanoparticles at the air-liquid interface: a comparison with conventional, submerged cell-culture conditions. BioMed. Res. Int. 2013, 1–12.

Luther, E.M., Schmidt, M.M., Diendorf, J., Epple, M., Dringen, R., 2012. Upregulation of metallothioneins after exposure of cultured primary astrocytes to silver nanoparticles. Neurochem. Res. 37 (8), 1639–1648 (Aug).

Martin, S., de Haan, L., Miro Estruch, I., Eder, K.M., Marzi, A., Schnekenburger, J., et al., 2022. Pre-validation of a reporter gene assay for oxidative stress for the rapid screening of nanobiomaterials. Front. Toxicol. 4, 974429. Sep 5.

Meldrum, K., Evans, S.J., Vogel, U., Tran, L., Doak, S.H., Clift, M.J.D., 2022. The influence of exposure approaches to *in vitro* lung epithelial barrier models to assess engineered nanomaterial hazard. Nanotoxicology 16 (1), 114–134. Jan 2.

Motta, G., Gualtieri, M., Saibene, M., Bengalli, R., Brigliadori, A., Carrière, M., et al., 2023. Preliminary toxicological analysis in a safe-by-design and adverse outcome pathway-driven approach on different silver nanoparticles: assessment of acute responses in A549 Cells. Toxics 11 (2), 195. Feb 20.

Raj, S., Jose, S., Sumod, U., Sabitha, M., 2012. Nanotechnology in cosmetics: opportunities and challenges. J. Pharm. Bioall Sci. 4 (3), 186.

Raudvere, U., Kolberg, L., Kuzmin, I., Arak, T., Adler, P., Peterson, H., et al., 2019. g: Profiler: a web server for functional enrichment analysis and conversions of gene lists (2019 update). Nucleic Acids Res. 47 (W1), W191–W198. Jul 2.

Sanchez-Guzman, D., Boland, S., Brookes, O., Mc Cord, C., Lai Kuen, R., Sirri, V., et al., 2021. Long-term evolution of the epithelial cell secretome in preclinical 3D models of the human bronchial epithelium. Sci. Rep. 11 (1), 6621 (Dec).

Servin, A., Elmer, W., Mukherjee, A., De la Torre-Roche, R., Hamdi, H., White, J.C., et al., 2015. A review of the use of engineered nanomaterials to suppress plant disease and enhance crop yield. J. Nanopart. Res 17 (2), 92 (Feb).

Smith, J.N., Thomas, D.G., Jolley, H., Kodali, V.K., Littke, M.H., Munusamy, P., et al., 2018. All that is silver is not toxic: silver ion and particle kinetics reveals the role of silver ion aging and dosimetry on the toxicity of silver nanoparticles. Part Fibre Toxicol. 15 (1), 47 (Dec).

Stebounova, L.V., Adamcakova-Dodd, A., Kim, J.S., Park, H., O'Shaughnessy, P.T., Grassian, V.H., et al., 2011. Nanosilver induces minimal lung toxicity or inflammation in a subacute murine inhalation model. Part Fibre Toxicol. 8 (1), 5 (Dec).

Sthijns, M.M., Thongkam, W., Albrecht, C., Hellack, B., Bast, A., Haenen, G.R., et al., 2017. Silver nanoparticles induce hormesis in A549 human epithelial cells. Toxicol. Vitr. 40, 223–233 (Apr).

Stucki, A.O., Barton-Maclaren, T.S., Bhuller, Y., Henriquez, J.E., Henry, T.R., Hirn, C., et al., 2022. Use of new approach methodologies (NAMs) to meet regulatory requirements for the assessment of industrial chemicals and pesticides for effects on human health. Front. Toxicol. 4, 964553. Sep 1.

Sung, J.H., Ji, J.H., Park, J.D., Yoon, J.U., Kim, D.S., Jeon, K.S., et al., 2009. Subchronic inhalation toxicity of silver nanoparticles. Toxicol. Sci. 108 (2), 452–461 (Apr).

Tyanova, S., Temu, T., Sinitcyn, P., Carlson, A., Hein, M.Y., Geiger, T., et al., 2016. The Perseus computational platform for comprehensive analysis of (prote)omics data. Nat. Methods 13 (9), 731–740 (Sep).

Val, S., Martinon, L., Cachier, H., Yahyaoui, A., Marfaing, H., Baeza Squiban, A., 2011. Role of size and composition of traffic and agricultural aerosols in the molecular responses triggered in airway epithelial cells. Inhal. Toxicol. 23 (11), 627–640 (Sep).

Vales, G., Rubio, L., Marcos, R., 2015. Long-term exposures to low doses of titanium dioxide nanoparticles induce cell transformation, but not genotoxic damage in BEAS-2B cells. Nanotoxicology 9 (5), 568–578.

Wang, L., Luanpitpong, S., Castranova, V., Tse, W., Lu, Y., Pongrakhananon, V., et al., 2011. Carbon nanotubes induce malignant transformation and tumorigenesis of human lung epithelial cells. Nano Lett. 11 (7), 2796–2803.

Xi, W.-S., Li, J.-B., Liu, Y.-Y., Wu, H., Cao, A., Wang, H., 2021. Cytotoxicity and genotoxicity of low-dose vanadium dioxide nanoparticles to lung cells following long-term exposure. Toxicology 459, 152859.

Yeyeodu, S.T., Martin, M.E., Reaves, D.K., Enders, J.R., Costantini, L.M., Fleming, J.M., 2019. Experimental data demonstrating the effects of silver nanoparticles on basement membrane gene and protein expression in cultured colon, mammary and bronchial epithelia. Data Brief. 26, 104464 (Oct).

Zhang, F., Aquino, G.V., Dabi, A., Bruce, E.D., 2019. Assessing the translocation of silver nanoparticles using an in vitro co-culture model of human airway barrier. Toxicol. Vitr. 56, 1–9.